Constitutive relations in 3-D for a wide range of strain rates and temperatures – Application to mild steels

A. Rusinek [a,*], R. Zaera [b], J.R. Klepaczko [a]

[a] *Laboratory of Physics and Mechanics of Materials, UMR CNRS 75 54, University of Metz, Ile du Saulcy, 57045 Metz cedex, France*
[b] *Department of Continuum Mechanics and Structural Analysis, University Carlos III of Madrid, Avda. de la Universidad 30, 28911 Leganés, Madrid, Spain*

Abstract

An original phenomenological thermo-visco-plastic model is reported that encompasses strain hardening, strain rate and temperature sensitivity. The model is based to some extent on the concept of physical modeling proposed earlier by Klepaczko [Klepaczko, J.R. 1975. Thermally activated flow and strain rate history effects for some polycrystalline FCC metals. Mater. Sci. Engng. 18, 121 135] , and also by different authors, for example: [Becker, R. 1925. Uber die plastizitat amorpher und kristalliner fester korper. Z. Physik 26, 919 925; Seeger, A., 1957. Dislocations and Mechanical Properties of Crystals, Wiley, New York; Conrad, H., 1964. Thermally activated deformation of metals J. Metals 16, 582; Gilman, J.J. 1968. Dislocation dynamics and response of materials to impact Appl. Mech. Rev. 21, 767 783; Gibbs, G.B., 1969. Thermodynamic analysis of dislocation glide controlled by dispersed local obstacles. Mater. Sci. Engng. 4, 313 328; Kocks, U.F., Argon, A.S., Ashby, M.F., 1975. Thermodynamics and kinetics of slip. In: Progress in Materials Science, vol. 19. Pergamon Press, New York, p. 19; Kocks, U.F. 1976. Laws for work-hardening and low-temperature creep. J. Eng. Mater. Technol. 98, 76 85, and later by many others.

The thermo-visco-plastic formulation, called RK and applied in this paper, has been verified experimentally for strain rates of $10^{-4}\ \mathrm{s}^{-1} \leqslant \dot{\bar{\varepsilon}}_{\mathrm{p}} \leqslant 5 \times 10^{3}\ \mathrm{s}^{-1}$ and temperatures $213\ \mathrm{K} \leqslant T \leqslant 393\ \mathrm{K}$, it covers the range of dynamic loadings observed during crash tests and other impact problems. In order to implement the RK constitutive relation, a thermo-visco-plastic algorithm based on the J_2 theory of plasticity is constructed. The type of algorithm is a return mapping one that introduces the consistency condition $(f = \bar{\sigma} - \sigma_y, f = 0)$, without the overstress state proposed by Perzyna [Perzyna, P. 1966. Fundamental problems in viscoplasticity. Advances in Applied Mechanics, vol. 9. Academic Press, New York, pp. 243 377]. The coupling of the RK constitutive relation with the integration scheme of the thermo-visco-plastic algorithm has demonstrated its efficiency for numerical analyses of different dynamic processes such as Taylor test [Zaera, R., Fernández-Sáez, J. 2006. An implicit consistent algorithm for the integration of thermoviscoplastic constitutive equations in adiabatic conditions and finite deformations. Int. J. Solids Struct., 43, 1594 1612.], ring expansion [Rusinek, A., Zaera, R., 2007. Finite element simulation of steel ring fragmentation under radial expansion. Int. J. Impact Eng. 34, 799 822], dynamic tension test [Rusinek, A., Zaera, R., Klepaczko, J.R., Cherigueme, R., 2005. Analysis of inertia and scale effects on dynamic neck formation during tension of sheet steel. Acta Mater. 53, 5387 5400], perforation of metallic sheets [Rusinek, A., 2000, Modélisation thermoviscoplastique d'une nuance de tôle d'acier aux grandes vitesses de déformation. Etude expérimentale et numérique du cisaillement, de la traction et de la perforation, Ph.D. thesis, University of Metz,

* Corresponding author. Tel.: +33 3 87 31 50 20; fax: +33 3 87 31 53 66.
E mail address: rusinek@lpmm.univ metz.fr (A. Rusinek).

France], and other cases. All the equations are implemented via the user subroutine VUMAT in the ABAQUS/Explicit code for adiabatic conditions of plastic deformation.

Keywords: Mild steel; RK Constitutive relation; Thermo visco plasticity; Consistent algorithm; Dynamic plasticity; Numerical simulat ions; Finite element code

1. Introduction

Behavior of materials at high strain rates and at different temperatures is of high priority in the sphere of crashworthiness. In order to understand the evolution of deformation fields and the mechanisms of failure at high loading rates, precise analytical and numerical tools are required. In this study, the prime interest is the quasi-static and dynamic behavior of the mild steel ES used in the automotive industry. The study of a specific material for a well-determined application, in this case the automobile crash, circumscribes the work area in terms of the effective stress σ, the effective plastic deformation ε_p, the effective strain rate $\dot{\varepsilon}_p$, and the temperature T (see Table 1). The reason for developing an advanced phenomenological approach is the ease with which this type of constitutive relation $\sigma = f(\varepsilon_p, \dot{\varepsilon}_p, T)$ may be introduced into finite element codes such as ABAQUS (2004). It is assumed that an adequate precision in material characterization can be achieved, as in the case of a physical formulation in which, for example, the evolution of dislocation density is taken into account. The difficulties of applying the physical formulation to finite element codes lies in a set of differential equations introduced to follow the evolution of the microstructure defined by one or more internal variables, then the constitutive relation is more complicated, for example $\sigma = f[\varepsilon_p, \dot{\varepsilon}_p, T, S_j(\varepsilon_p, \dot{\varepsilon}_p, T)]$, where S_j is a set of j internal state variables. It is clear however that with the phenomenology approach a simplification can be arranged more precisely on the basis of physical notions leading to a constitutive relation of the form $\sigma = f(\varepsilon_p, \dot{\varepsilon}_p, T)$. This is an approach defined as the Mechanical Equation of State (MES) with absence of strain rate and temperature history effects, Klepaczko and Duffy (1982). Here, a comparison is also made between the proposed constitutive relation, called RK, and other formulations, such as Johnson and Cook (1983) or Cowper and Symonds (1952), implemented originally into commercial finite element codes. However, many others constitutive relations are frequently used to simulate dynamic processes. The most common approach is that derived via analogy to dislocation dynamics, for example Zerilli and Armstrong (1987). The previous list is not exhaustive and comparison between several formulations was discussed by Liang and Khan (1999).

Another group of constitutive relations, without assumption of the MES, is based on hypothetical evolution of the rate of strain hardening, $\theta = g(\varepsilon_p, \dot{\varepsilon}_p, T)$, where $\theta = d\sigma/d\varepsilon_p$. Some typical examples in that group are constitutive relations introduced for example by Bodner and Partom (1975), Kocks (1976), Klepaczko (1987, 1994), more recently by Molinari and Ravichandran (2005) and also others. The best example is the Mechanical Threshold Stress (MTS) model, Follansbee and Kocks (1988). The main problem with this concept is a serious difficulty in formulation of a precise explicit mathematical form of the evolution of strain hardening rate θ with plastic strain, strain rate and temperature. Even if this task is accomplished correctly the integration of the differential equation with a complex g-function leads to non-closed form solutions for stress. In addition, the current values of strain hardening rate must be always updated during numerical integration. Therefore the CPU may be much extended in more complicated engineering problems. In conclusion, the RK

Table 1
Classification of the processes as a function of the strain rates in terms of inertia and thermal coupling

Applications	$\dot{\varepsilon}_p(s^{-1})$	Inertia	Thermal processes
Static	$<10^{-4}\ s^{-1}$		
Punching, cutting ...	$10^{-3}\ s^{-1}$ $10^{2}\ s^{-1}$	Negligible	Isothermal
Crash test	$1\ s^{-1}$ $5*10^{2}\ s^{-1}$	Important	Adiabatic
High speed machining, ballistic, impact, ring expansion...	Up to $10^{3}\ s^{-1}$		

constitutive relation presented in this paper is limited to the MES with a possibility to apply standard material model subroutines available in many commercial computer codes.

2. Analysis of the thermo-visco-plastic behavior of a mild steel

The behavior of mild steel reported in this paper can be assumed as a reference since it has been analyzed by several laboratories in the last decade. It is the cold rolled mild steel after an annealing to reduce the rolling effect that causes residual stresses and anisotropy. Elements such as aluminum and titanium are added in small proportion (<0.1wt%) to produce fine-grained material and formation of carbides to increase the failure stress level (see Table 2). After rolling and annealing the average grain size obtained by the image correlation was ϕ 16 μm. The distribution of length to width of grains showed the characteristic elliptic grain shape oriented along the rolling direction. Those microscopic observations were performed to gain some knowledge on anisotropy caused by geometric and spatial grain distribution. Of course, there is also an anisotropy effect related to the crystallographic texture and microstructure. In addition to several metallurgical analyses, the tension tests were performed in two directions, complementary to the rolling direction, that is φ_1 45° and φ_2 90°. No effect of rolling direction was found on the macroscopic behavior even if the grain shape was not equi-axial. For the reasons given above, the isotropy is assumed in the description of the material behavior, and the J_2 theory is applied as in 3D generalization by Zaera and Fernández-Sáez (2006).

To complete the dynamic and quasi-static testing, the tension tests were performed at room temperature. The temperature tests were performed in $213\ \mathrm{K} \leqslant T_0 \leqslant 373\ \mathrm{K}$ at different strain rates $10^{-5}\ \mathrm{s}^{-1} \leqslant \dot{\varepsilon}_\mathrm{p} \leqslant 10^{-1}\ \mathrm{s}^{-1}$. The final results are shown in Fig. 1 in the form of the nominal stress versus the nominal strain, $\sigma_n(\varepsilon_n)$. The first observation is an increase of the strain rate sensitivity as temperature decreases, more precisely when the temperature is between RT (room temperature) and T_0 213 K, inducing at the same time a decrease of ductility, $\varepsilon_n < 0.1$ at strain rate $\dot{\varepsilon}_\mathrm{p} \geqslant 10^{-1}\ \mathrm{s}^{-1}$. The substantial increase of stress with strain rate at low temperatures allows determination of the transition between the athermal and thermally activated states of strain hardening. In fact, the reciprocity strain rate/temperature may be defined and analyzed. It is well known that an increase of strain rate is equivalent to a reduction of temperature, therefore, when the test temperature is lowered, the strain rate to reach the thermal activation process is reduced. This reciprocity is the foundation of the physical modeling based on the processes of thermal activation. The $T-\dot{\varepsilon}$ relation applied in constitutive modeling by many authors is generally expressed by the Arrhenius equation, Eq. (1), combined with the frequency factor, Eq. (2), Klepaczko (1987). The relation between strain rate and temperature within the thermally activated regime of plastic deformation can be evaluated directly from the standard Arrhenius relation, Conrad (1964)

$$\dot{\varepsilon}_\mathrm{p} = \dot{\varepsilon}_0 \exp\left(-\frac{\Delta G(\sigma^*)}{kT}\right) \tag{1}$$

$$\dot{\varepsilon}_0 = n\rho_\mathrm{m} b^2 v_\mathrm{D} \tag{2}$$

where ρ_m is the density of mobile dislocations, n is the kink geometry factor, b is the modulus of Burgers vector, v_D is the Debye frequency, ΔG is the free energy of activation, k is the Boltzmann constant and σ^* the effective stress (Peierls stress in BCC lattices) related to the strain rate and temperature. The frequency factor $\dot{\varepsilon}_0 = n\rho_\mathrm{m} b^2 v_\mathrm{D}$ is directly related to the mobile dislocation density ρ_m. The transition point $(\dot{\varepsilon}_\mathrm{p}^{\mathrm{tr}}, T_{\mathrm{tr}})$ from the thermally activated plastic flow to ''athermal'' state is defined when the effective stress is ceased, that is when σ^* 0.

The strain rate-temperature equivalence forms the basis of the semi-phenomenological RK constitutive model (Rusinek and Klepaczko, 2001). The effective stress σ^* defines variation of flow stress due to thermally

Table 2
Chemical composition of the mild steel ES (% of wt)

Mn	Al	Cr	C	Ni	S	Cu	Si	P	N	Ti
0.203%	0.054%	0.041%	0.03%	0.018%	0.011%	0.009%	0.009%	0.008%	0.0063%	0.002%

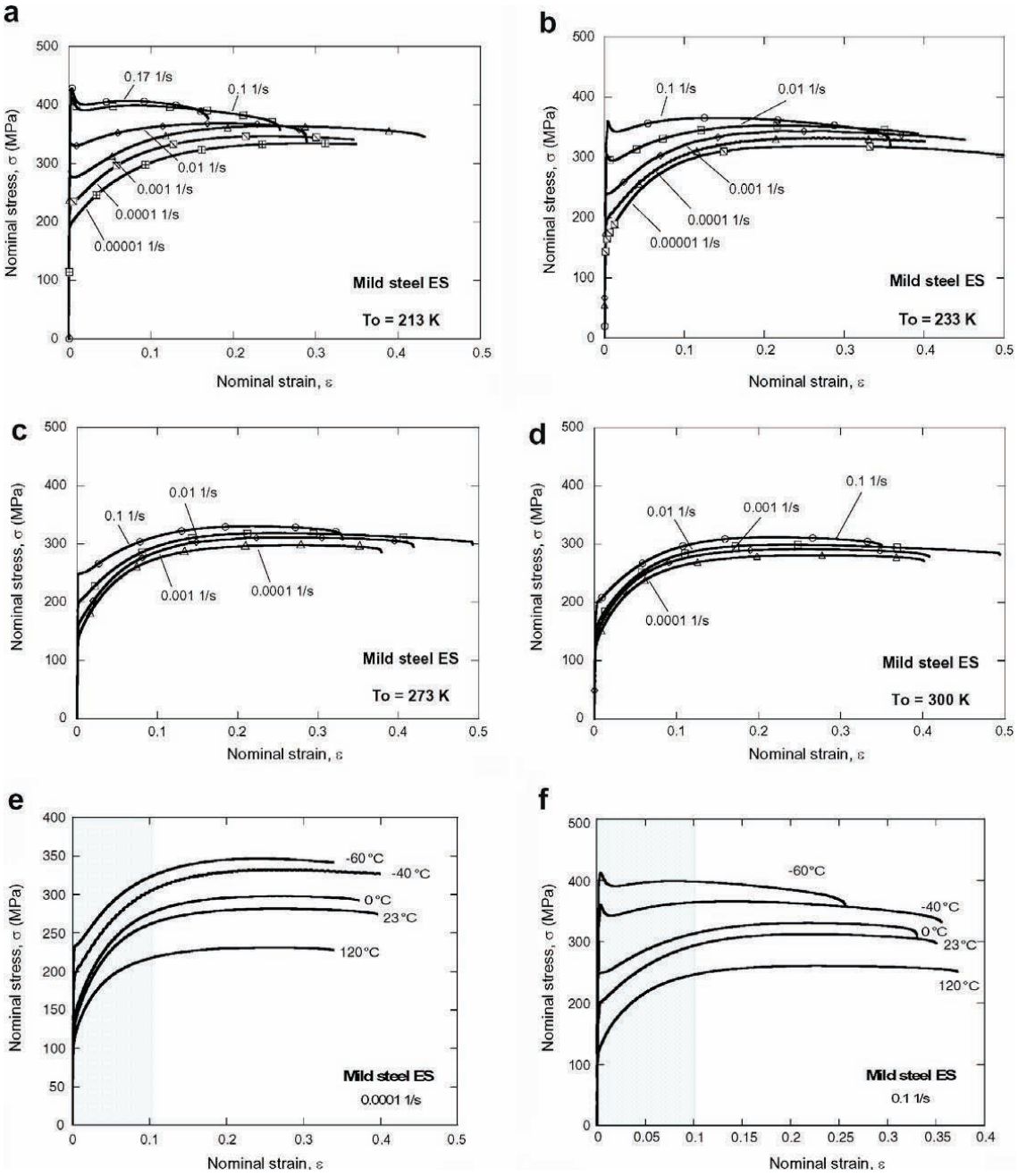

Fig. 1. (a d) Effect of the initial temperature on the strain rate sensitivity, definition of the reciprocity strain rate/temperature for mild steel design ES, (e f) Effect of initial temperature for different strain rates.

activated dislocation dynamics at different strain rates and temperatures. This effect is caused by dislocation jumping over the thermally activated short-distance obstacles (Conrad, 1964). In the BCC lattice this is the Peierls potential. If an explicit relation $\Delta G(\sigma^*)$ is known then Eq. (1) can be inverted and the effective stress determined. In the non-linear approach, which is suitable for BCC metals, the free energy of activation is given by Kocks et al. (1975),

$$\Delta G = \Delta G_0 \left[1 - \left(\frac{\sigma^*}{\sigma_0^*} \right)^p \right]^q \tag{3}$$

where ΔG_0 is the average activation free energy required to overcome a local obstacle without applied stress and p and q are geometric parameters which define the shape of obstacles. Generally, the values used for p and q are $0 \leqslant p \leqslant 1$ and $1 \leqslant q \leqslant 2$ (Gilman, 1968; Klepaczko, 1981; Kocks et al., 1975; Hoge and Mukherjee, 1977; Uenishi and Teodosiu, 2004). If the effective stress is zero then $\Delta G \quad \Delta G_0$. Substitution of Eq. (3) into Eq. (1) yields the explicit form for the effective stress:

$$\sigma^* = \sigma_0^* \left\{ 1 - \left[\frac{kT}{\Delta G_0} \ln \left(\frac{\dot{\varepsilon}_0}{\dot{\varepsilon}_p} \right) \right]^{1/q} \right\}^{1/p} \tag{4}$$

The transition to the "athermal" mode of plastic flow is defined by posing $\sigma^* = 0$, then

$$\sigma_0^* \left\{ 1 - \left[\frac{kT_{tr}}{\Delta G_0} \ln \left(\frac{\dot{\varepsilon}_0}{\dot{\varepsilon}_p^{tr}} \right) \right]^{1/q} \right\}^{1/p} = 0 \quad \text{and} \quad \dot{\varepsilon}_p^{tr} = n\rho_m b^2 v_D \exp\left(-\frac{\Delta G_0}{kT_{tr}} \right) \tag{5}$$

According to Seeger (1957) the total flow stress is composed of two parts, the effective stress σ^* and the "athermal" stress component σ_μ, then $\sigma = \sigma_\mu + \sigma^*$. In general, due to more complex dislocation processes both stress components depend on strain, strain rate and temperature, (Klepaczko, 1975), then

$$\sigma(\varepsilon_p, \dot{\varepsilon}_p, T) = \sigma_\mu(\varepsilon_p, \dot{\varepsilon}_p, T) + \sigma^*(\varepsilon_p, \dot{\varepsilon}_p, T) \tag{6}$$

For $\dot{\varepsilon}_p \leqslant \dot{\varepsilon}_p^{tr}$ and $T \geqslant T_{tr}$, Eq. (6) reduces to the following form

$$\sigma(\varepsilon_p, \dot{\varepsilon}_p, T) = \sigma_\mu(\varepsilon_p, \dot{\varepsilon}_p, T) \tag{7}$$

In Eq. (6) the effective stress depends also on plastic strain. This is caused by the fact that the evolution of the mobile dislocation density depends on the evolution of plastic strain. The strain hardening is assumed in Eq. (6) in the form of MES. Therefore, Eq. (6) constitutes the fundamental base, supported by some physical processes of plastic deformation, in construction of the RK constitutive relation (Rusinek and Klepaczko, 2001). The internal stress is discussed more exactly in the further part of this paper.

Combining all the experimental results obtained for the ES steel, it is possible to estimate the transition strain rate with the initial temperature applied during the tests. The effect of the strain rate at different temperatures is shown in Fig. 1. In general, the logarithmic strain rate sensitivity m is defined by Eq. (8).

$$m = \left(\frac{\partial \log \sigma}{\partial \log \dot{\varepsilon}^p} \right)_{\varepsilon_p, T} \tag{8}$$

In mild steels, the mean value of m is considered constant and equal to $m \approx 0.02$. In the present case, the value of m found at room and higher temperatures is close to this value, Fig. 2a and b. However, at low temperatures, $T < 300$ K, a strong increase of the logarithmic rate sensitivity is observed with maximum value $m_{max} \quad 0.044$ at $T \quad 213$ K, Fig. 2a and b. This phenomenon of high strain rate sensitivity is more important at low temperatures in the same range of strain rates, as it can be seen in Fig. 2b ($m_{low\ T} \gg m_{room\ T}$). A substantial increase of the rate sensitivity at low temperatures for BCC metals is related to the thermally activated Peierls potential, see for example the works of Conrad (1964) and Klepaczko (1994).

It is clear from this observation that the coupling $T - \dot{\varepsilon}_p$ is essential in a correct definition of the transition between the "athermal" and thermally activated processes of plastic deformation, notably at low temperatures, but also at high strain rates above room temperature. This effect of the transition from "athermal" to thermal activation is demonstrated in Fig. 3a and b; the strain rate transition at room temperature is observed to be in the range $10\ s^{-1} < \dot{\varepsilon}_p \leqslant 100\ s^{-1}$ (Rusinek, 2000; Nowacki, 2001; Mourro, 2002) and in the range $10^{-2}\ s^{-1} < \dot{\varepsilon}_p \leqslant 10^{-1}\ s^{-1}$ at $T \quad 213$ K, Fig. 2a. It can be also observed that the strain rate sensitivity at room temperature is not constant, Fig. 3a and b. Three characteristic regions how the rate sensitivity varies were reported by Campbell and Ferguson (1970). The comparison between the experimental data and various constitutive relations is discussed in the next section. The comparison is given in terms of true stress and true strain obtained in tension by use of the standard relations. The definition of the true strain takes into account the diminution of the cross-sectional area of the specimen during plastic deformation. The cross-section

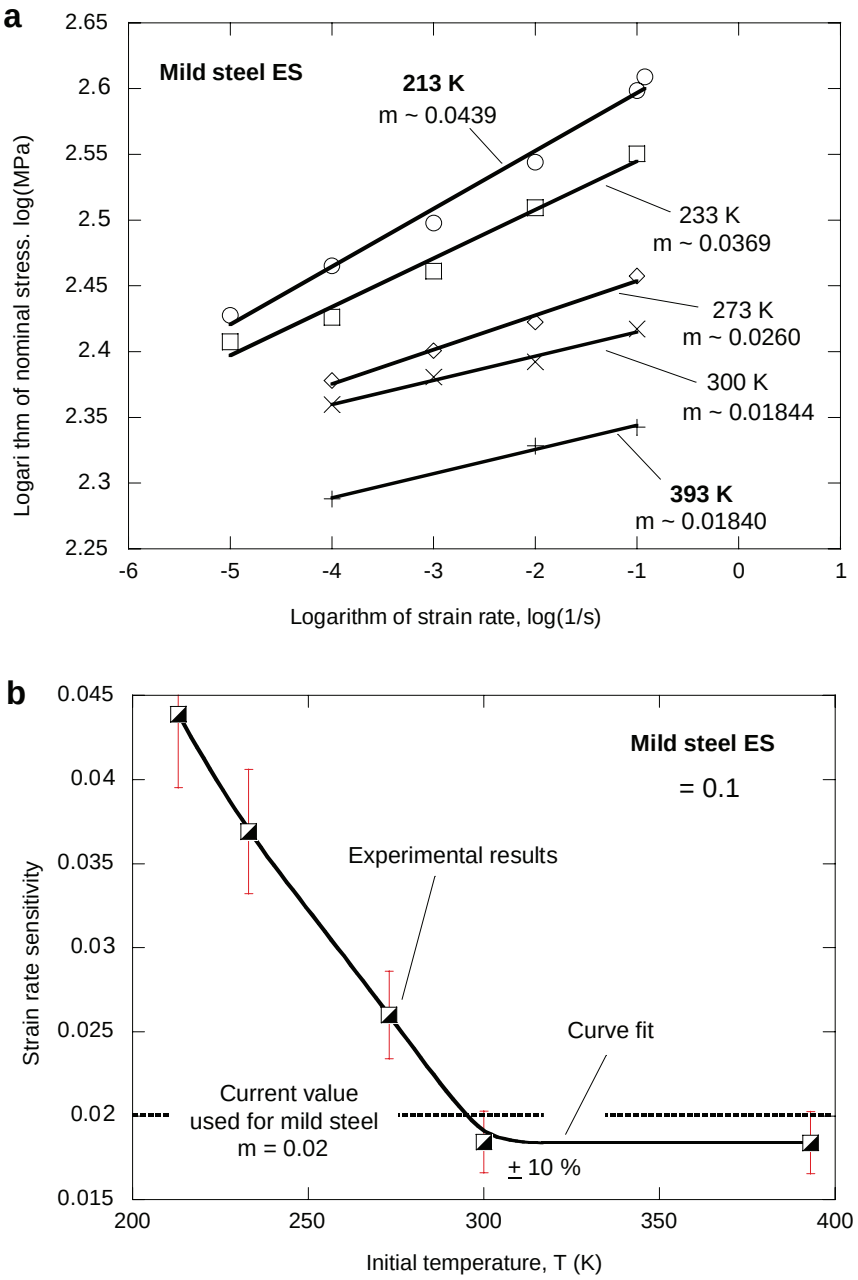

Fig. 2. (a) Effect of the initial temperature on the logarithm strain rate sensitivity of mild steel ES, 213 K $\leqslant T \leqslant$ 393 K and (b) evolution of strain rate sensitivity m with the initial temperature at an imposed plastic strain.

reduction gives rise to necking and the loss of homogeneity of plastic deformation. The experimental curves in the form of true stress versus true strain obtained at different temperatures and strain rates can be used to identify the material constants in the RK constitutive relation. The procedure of identification is valid up to the true strain level $\varepsilon^{p}_{\max}$ when the following generalized criterion is reached, which is defined by Eq. (9)

$$\sigma = \left.\frac{\partial\sigma}{\partial\varepsilon_{\mathrm{p}}}\right|_{\varepsilon_{\mathrm{p}},T} \quad \text{or} \quad \sigma\left(\varepsilon_{\mathrm{p}},\dot{\varepsilon}_{\mathrm{p}},T\right) = \theta\left(\varepsilon_{\mathrm{p}},\dot{\varepsilon}_{\mathrm{p}},T\right) \tag{9}$$

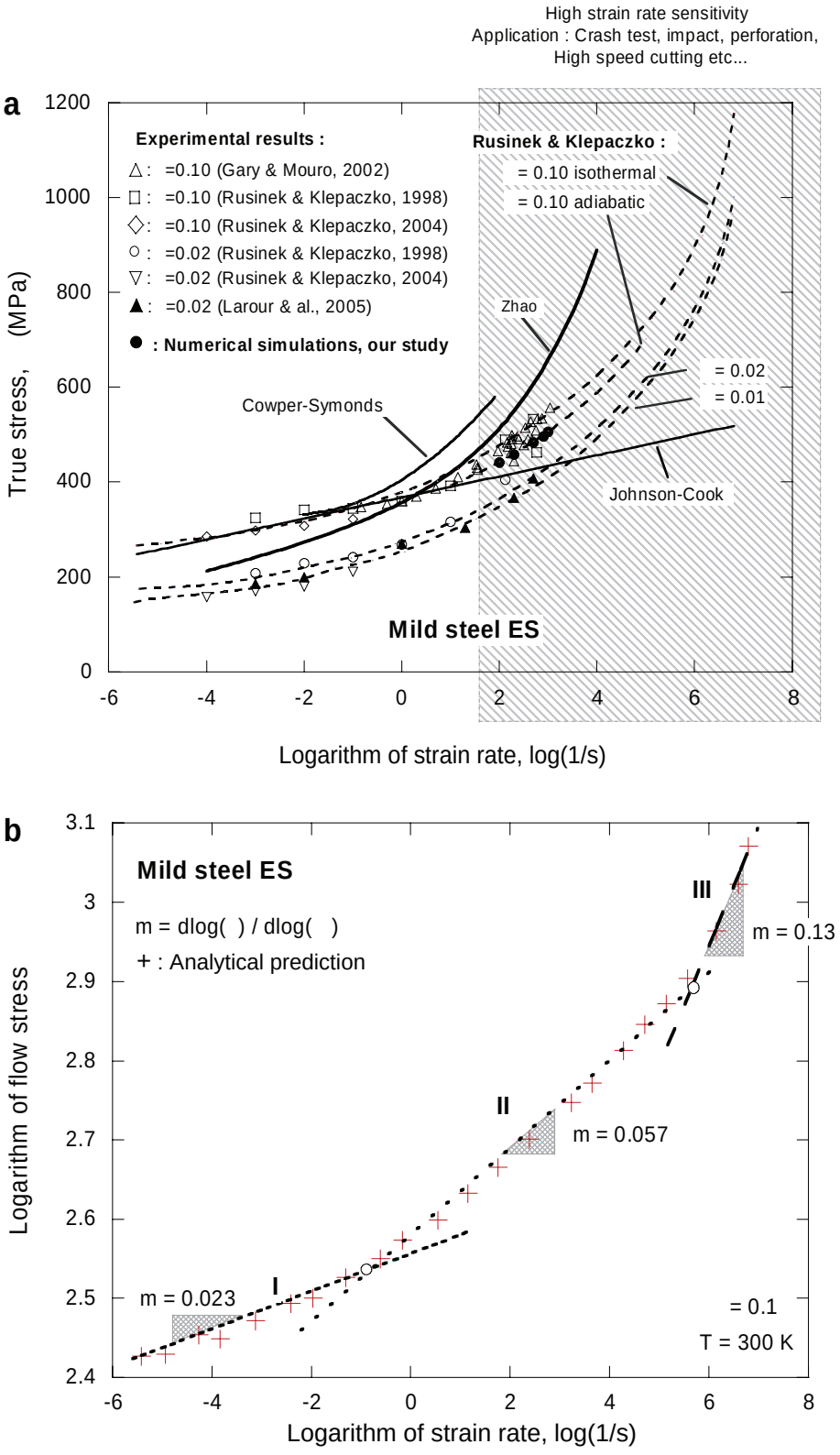

Fig. 3. (a) Strain rate sensitivity for different plastic strain and for different deformations at room temperature. Comparison of some constitutive relations and RK constitutive relation with experimental results and (b) variation of the strain rate sensitivity at room temperature within three characteristic regions, according to Campbell and Ferguson (1970).

This is the generalized Considère (1885) criterion by Klepaczko (1968). The RK constitutive relation used in this paper is based on several papers published by Klepaczko and cited in the references. The RK relation takes into account (to some extent) the theory of dislocation dynamics. Here, the relation neglects the microstructural parameters and does not include the evolution of the internal microstructure during plastic deformation. However, this formulation has a sound basis, like the internal and effective stress components, more particularly related to the processes of thermal activation, including behavior at high strain rates, $\dot{\varepsilon}_p \geqslant 100\ s^{-1}$.

3. Discussion of the RK thermo-visco-plastic constitutive relation

At present several constitutive relations are available to predict by FE the distribution of plastic deformation and failure in structures under impact. Some of them are limited to perfectly plastic approximations with a visco-plasticity. More sophisticated versions such as with thermo-visco-plasticity and strain hardening are also available nowadays. In the last case the plastic flow is a function of strain hardening, strain rate and temperature. Of course, the main task is to approximate precisely the response of engineering structures under impact. The RK constitutive relation is used because the precise constitutive modeling can predict the loading rate effects in terms of strain rate and temperature sensitivity. The final task was implementation of the RK constitutive relation into a finite element code to simulate dynamic processes related to crash tests.

In order to describe the plastic flow of mild steel ES, the observation based on materials science is applied so that the total stress in BCC microstructures is additive in the form of the internal and effective stress components. The unique feature of this constitutive relation is an assumption that the strain hardening is rate and temperature sensitive. In the case of steels, when the strain rate $\dot{\varepsilon}$ increases a decrease of the rate of strain hardening is observed at the same time. This is due to dislocation multiplication and thermal softening. In the RK formulation, by similarity to the physical models, for example (Seeger, 1957; Klepaczko, 1975; Kocks, 1976; Meyers et al., 2002), is assumed that the total stress is the sum of two components, the internal stress σ_μ and the effective stress σ^*.

$$\sigma\left(\varepsilon_p, \dot{\varepsilon}_p, T\right) = \frac{E(T)}{E_0}\left[\sigma_\mu(\varepsilon_p, \dot{\varepsilon}_p, T) + \sigma^*(\dot{\varepsilon}_p, T)\right] \tag{10}$$

The first term is directly related to the strain hardening of the material and the second defines the stress contribution due to the thermal activation (combination of temperature and strain rate). Because of the thermal softening of crystalline lattice the both stress components are normalized by temperature-dependent Young's modulus $E(T)$, Fig. 4. The expression for $E(T)$ is based to some extent on physical considerations (Klepaczko, 1994), and is given by:

$$\frac{E(T)}{E_0} = 1 - \frac{T}{T_m}\exp\left(\theta^*\left(1 - \frac{T_m}{T}\right)\right) \tag{11}$$

where θ^* is the characteristic homologous temperature.

The explicit forms for the two stress components are given by Eqs. (12)–(14) and (16). The originality of the expression for the internal stress σ_μ representing strain hardening is an introduction of temperature and strain rate effects via the plasticity modulus $B(\dot{\varepsilon}_p, T)$ and the strain hardening exponent n, that is $n(\dot{\varepsilon}_p, T)$. This is postulated by Eq. (12). The latter comes from many experimental observations for steels. Therefore the internal stress is given by

$$\sigma_\mu(\varepsilon_p, \dot{\varepsilon}_p, T) = B(\dot{\varepsilon}_p, T)\left(\varepsilon_0 + \varepsilon_p\right)^{n(\dot{\varepsilon}_p, T)} \tag{12}$$

In Eq. (12) ε_0 is the strain at the yield stress when $\varepsilon_p = 0$, $B(\dot{\varepsilon}_p, T)$ and $n(\dot{\varepsilon}_p, T)$ are respectively the modulus of plasticity and the strain hardening exponent. The explicit expressions for the modulus of plasticity and strain hardening exponent are defined as follows, Eqs. (13) and (14)

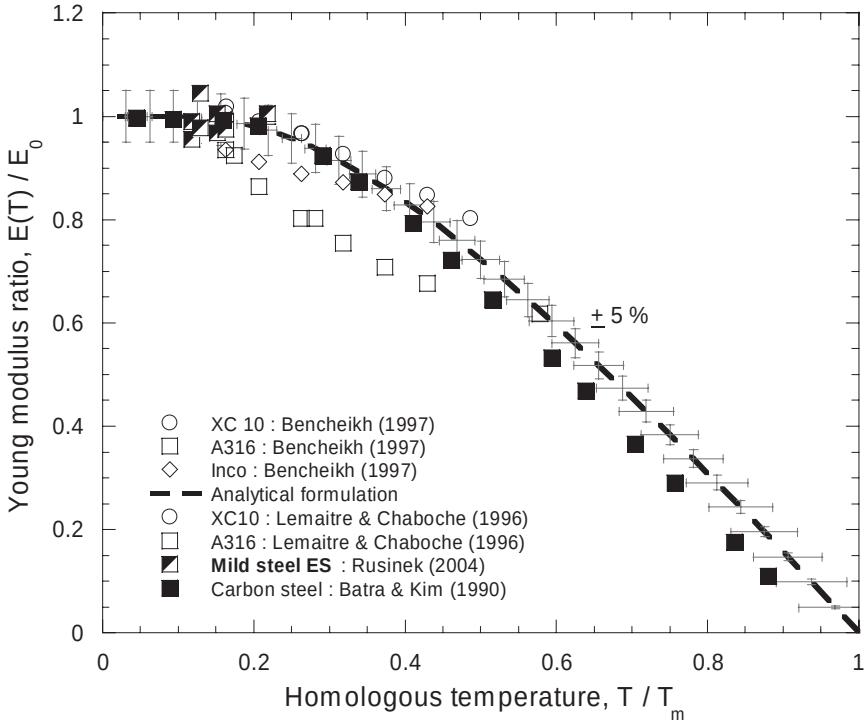

Fig. 4. Analytical prediction of temperature variation of Young's modulus and comparison for several kinds of steel.

$$B(\dot{\varepsilon}_{\mathrm{p}}, T) = B_0 \left[\left(\frac{T}{T_{\mathrm{m}}} \right) \log \left(\frac{\dot{\varepsilon}_{\max}}{\dot{\varepsilon}_{\mathrm{p}}} \right) \right]^{v} \tag{13}$$

$$n(\dot{\varepsilon}_{\mathrm{p}}, T) = n_0 \left(1 - D_2 \left(\frac{T}{T_{\mathrm{m}}} \right) \log \left(\frac{\dot{\varepsilon}_{\mathrm{p}}}{\dot{\varepsilon}_{\min}} \right) \right) \quad \text{with} \quad n(\dot{\varepsilon}_{\mathrm{p}}, T) \geqslant 0 \tag{14}$$

where n_0 is the strain hardening exponent at $T \quad 0$ K, D_2 is the material constant, $\dot{\varepsilon}_{\max}$ and $\dot{\varepsilon}_{\min}$ are respectively the maximum and minimum strain rates assumed in the model, B_0 is the plasticity modulus at $T \quad 0$, the constant v characterizes the temperature sensitivity of flow stress, T_{m} is the melting point.

A restriction is imposed on the strain hardening exponent, Eq. (14). Negative values of the strain hardening exponent n are not allowed in the present case. In fact, a negative value of the strain hardening exponent $n(\dot{\varepsilon}_{\mathrm{p}}, T)$ resulting from the temperature increase ΔT at an imposed strain rate $\dot{\varepsilon}^{p}$ would induce an increase of the stress level during plastic deformation, Fig. 5b, whereas in general case the material must soften. Such effect is in contradiction to the physical observations in steels (with exception of Dynamic Strain Ageing – DSA). A temperature increase generally induces a decrease of strain hardening rate and also the stress level. Therefore this restriction must be imposed automatically in finite element calculations, that is $n(\dot{\varepsilon}_{\mathrm{p}}, T) \geqslant 0$.

$$1 - D_2 \left(\frac{T}{T_{\mathrm{m}}} \right) \log \left(\frac{\dot{\varepsilon}_{\mathrm{p}}}{\dot{\varepsilon}_{\min}} \right) \geqslant 0 \quad \forall \quad \dot{\varepsilon}_{\mathrm{p}}, T \tag{15}$$

If the argument in Eq. (14) is negative, then $n \quad 0$ and the limit is the ideal plasticity. The limiting strain rate $\dot{\varepsilon}_{\mathrm{p}}^{c}$ for $n \quad 0$ can be obtained experimentally, and its value is usually high.

The effective stress $\sigma^{*}(\dot{\varepsilon}_{\mathrm{p}}, T)$ in the RK formulation is the simplified form of Eq. (4) based on the thermal activation strain rate plasticity. This stress component is given by

$$\sigma^{*}(\dot{\varepsilon}_{\mathrm{p}}, T) = \sigma_0^{*} \left[1 - D_1 \left(\frac{T}{T_{\mathrm{m}}} \right) \log \frac{\dot{\varepsilon}_{\max}}{\dot{\varepsilon}_{\mathrm{p}}} \right]^{1/m} \tag{16}$$

where $m^{*} \quad 1/m$ is the coefficient of the effect of temperature and strain rate on the effective stress, D_1 is the material constant, σ_0^{*} is the effective stress at $T \quad 0$ K, T_{m} is the melting point and $\dot{\varepsilon}_{\max}$ is the maximum strain

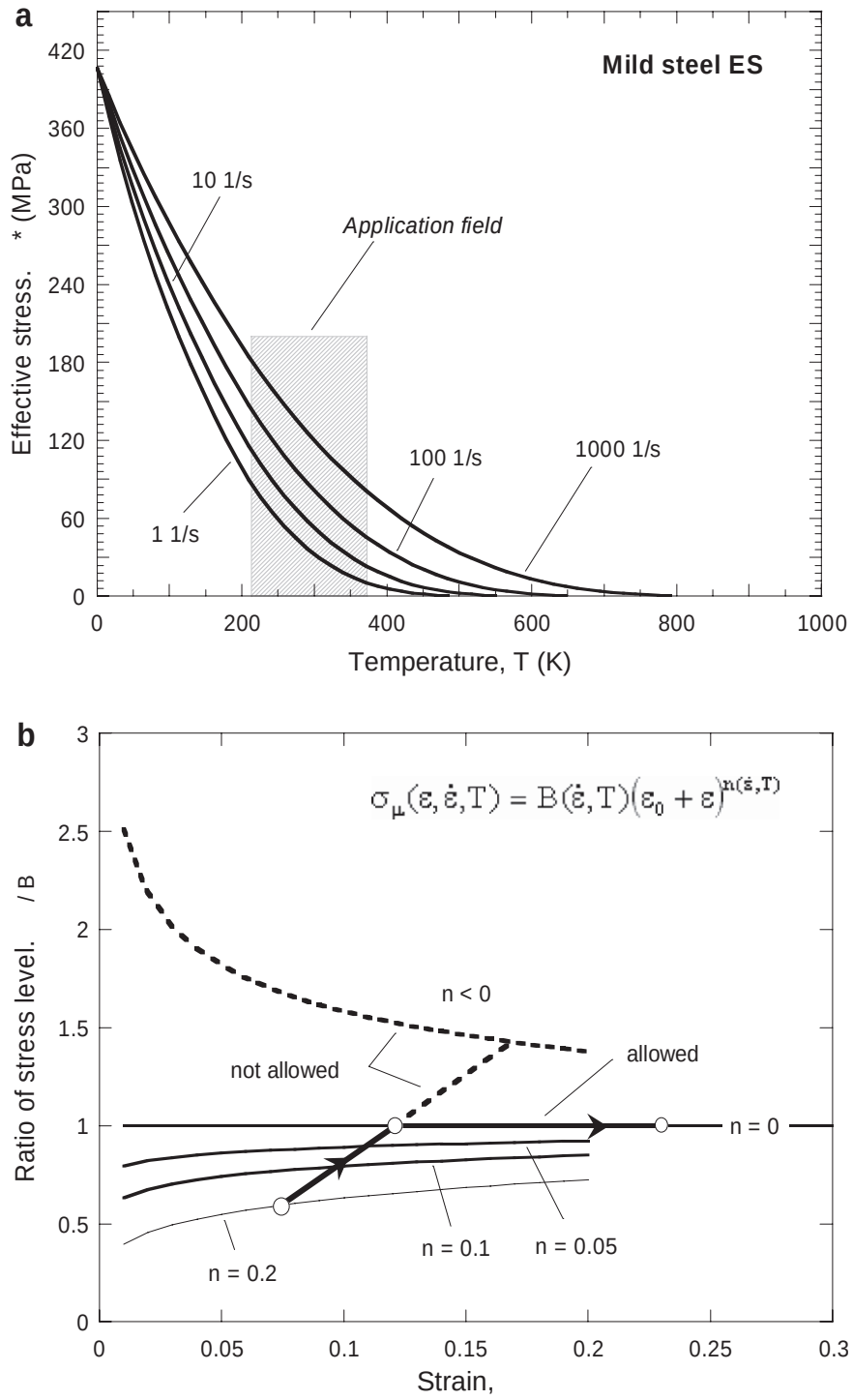

Fig. 5. (a) Effect of strain rate on the effective stress with temperature and (b) effect of the hardening exponent $n(\dot{\varepsilon}_p, T)$ on the internal stress σ_μ during plastic deformation, and definition of the upper limit of $n(\dot{\varepsilon}_p, T)$.

rate limiting validity of the equation. Another limit is the lowest strain rate when $\sigma^* = 0$ at specific temperature. The condition is defined below:

$$1 - D_1 \left(\frac{T_c}{T_m} \right) \log \left(\frac{\dot{\varepsilon}_{max}}{\dot{\varepsilon}_p^c} \right) \geqslant 0 \tag{17}$$

with the transition point $(\dot{\varepsilon}_p^c, T_c)$. If $\dot{\varepsilon}_p \leqslant \dot{\varepsilon}_p^c$ and $T \geqslant T_c$ then $\sigma^*(\dot{\varepsilon}_p, T) = 0$. It should be noted that the constant D_1 must be determined in such a way that the effective stress is zero at low strain rate reached during experiments, typically $\dot{\varepsilon}_p = 10^{-4}\ s^{-1}$ in Eq. (17). In this case, the evolution of stress is defined only by the internal stress σ_μ representing the contribution of strain hardening without thermal activation. The temperature evolution of the effective stress is manifested by a decreasing function of temperature.

Combination of the two stress components yields the thermal softening of material during temperature increase due to the conversion of plastic work into heat. The temperature effect on the effective stress σ^* is shown for several strain rates in Fig. 5a. This figure shows that at higher temperatures and lower strain rates the contribution of the effective stress σ^* is more limited.

To calculate the adiabatic increase of temperature, ΔT_A, resulting from the plastic work converted into heat, the balance of energy, Eq. (18), must be coupled with the complete form of the constitutive relations, Eq. (13)–(16). Neglecting the adiabatic increase of temperature that occurs at high strain rates will cause a rise of strain hardening during the process of plastic deformation and will not allow to study properly the problems of plastic instabilities such as the formation and propagation of adiabatic shear bands, Batra and Kim (1990). The adequate equation for the adiabatic increase of temperature is given by

$$T_A = T_0 + \Delta T_A \quad T_A = T_0 + \frac{\beta}{\rho C_p}\int_0^{\varepsilon_p} \sigma\left[\xi, \dot{\xi}(\xi), T\right] d\xi \tag{18}$$

where T_0 is the initial temperature, ρ is the density, C_p is the specific heat at constant pressure (assumed constant during numerical simulation) and β is the Taylor–Quinney coefficient which may vary with plastic deformation (Macdougall, 2000; Hodowany et al., 2000). Here the constant value has been assumed, β 0.9.

A comparison of the RK analytical predictions with experimental results obtained for ES steel is shown in Fig. 6a–f. There is good agreement between stress predictions and experiments for this steel. The second observation is a small effect of temperature on Young's modulus at temperatures below room temperature. However at high temperatures, the decrease of Young's modulus $E(T)$ is very pronounced, this causes a decrease of the elastic wave speed with the rise of temperature.

With the specified set of constitutive equations, and after identification of the material constants by an algorithm that begins with the starting point defined by the lowest critical strain rate and the lowest critical temperature (Rusinek, 2000), the algorithm is based on an optimization method of least squares. The comparison between experimental results and analytical predictions as it is shown in Fig. 6a–f , leads in general to good approximations by RK model. The comparison is obtained in the form of true stress and true plastic strain at different strain rates and in isothermal and adiabatic conditions. The material constants are given in Table 3a. In addition to the plots obtained for the RK constitutive relations, the $\sigma(\varepsilon)$ plots for the Johnson–Cook relation are given. At higher strain rates the $\sigma(\varepsilon)$ curves are adiabatic.

Very good agreement is obtained between the RK approximations and experiments for entire strain rate range presented in Fig. 6, $10^{-3}\ s^{-1} \leqslant \dot{\varepsilon}_p \leqslant 130\ s^{-1}$. A more detailed comparison is given elsewhere, for both tension and shear up to maximum strain rate close to $5 \times 10^3\ s^{-1}$, (Rusinek, 2000; Rusinek and Klepaczko, 2001). A comparison is shown in Fig. 7 between the predicted temperature effect and experimental data at two strain rates, $\dot{\varepsilon}_p = 10^{-3}\ s^{-1}$ and $\dot{\varepsilon}_p = 10^{-1}\ s^{-1}$, which were selected for the ease of reaching them experimentally. A relatively wide range of temperatures was applied using a temperature chamber with a standard quasi-static universal machine. More recently, the RK constitutive relation has also been analyzed to define accurately the material constants for different kind of new steels frequently used in automotive industries, DP600 (Larour et al., 2005), TRIP 700 (Larour et al., 2007), H340LAD (Larour et al., 2007), CMnAl-TRIP (Van Slycken et al., 2006), IF (see Appendix, Fig. A1) and HSLA-65 (see Appendix, Fig. A2). The constants for two additional materials are given in the appendix to proof the validity of the model for wide range of strain rates and also for a pre-strained material at different rates.

In addition to those experimental validations, the RK constitutive relation was compared with various models commonly used and pre-implemented in commercial finite element codes. This was done in order to simulate dynamic processes, for example by application of the Johnson and Cook (1983) relation, Eq. (19), Table 3b and the Cowper and Symonds (1952) constitutive equation, Eq. (20).

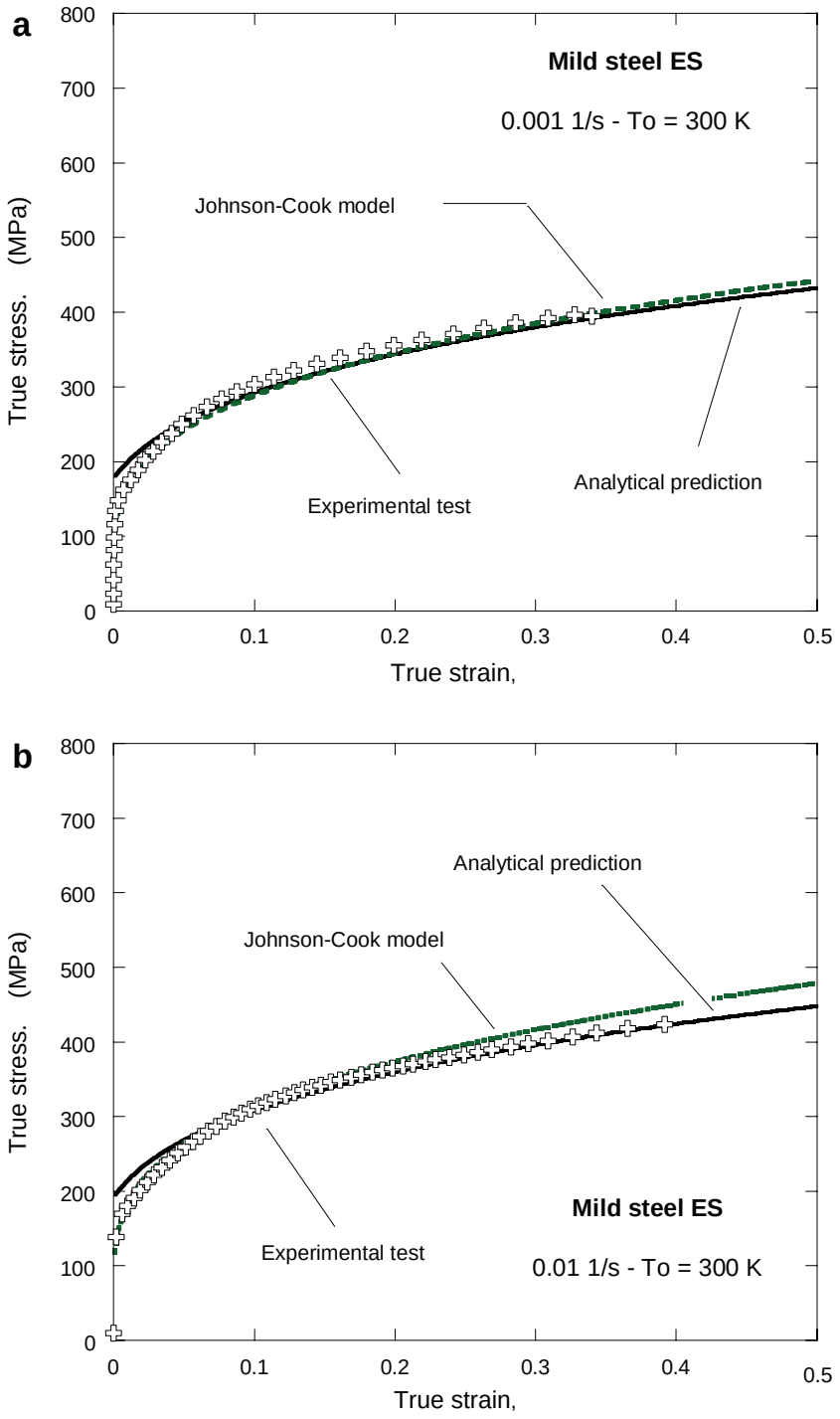

Fig. 6. Comparison of RK model predictions with experimental results at indicated initial temperatures and at different initial strain rates: (a) $10^{-3}\ \mathrm{s}^{-1}$, (b) $10^{-2}\ s^{-1}$, (c) $10^{-1}\ \mathrm{s}^{-1}$, (d) $1\ \mathrm{s}^{-1}$, (e) $10\ \mathrm{s}^{-1}$ and (f) $130\ \mathrm{s}^{-1}$.

$$\sigma\left(\varepsilon_{\mathrm{p}}, \dot{\varepsilon}_{\mathrm{p}}, T\right) = \left(A + B\left(\varepsilon_{\mathrm{p}}\right)^{n}\right)\left(1 + C\ln\left(\frac{\dot{\varepsilon}_{\mathrm{p}}}{\dot{\varepsilon}_{0}}\right)\right)\left(1 - \left(T^{*}\right)^{m}\right) \tag{19}$$

$$\sigma_{\mathrm{dyn}}\left(\dot{\varepsilon}_{\mathrm{p}}\right) = \sigma_{\mathrm{sta}}\left(1 + \left(\frac{\dot{\varepsilon}_{\mathrm{p}}}{D}\right)^{1/p}\right) \tag{20}$$

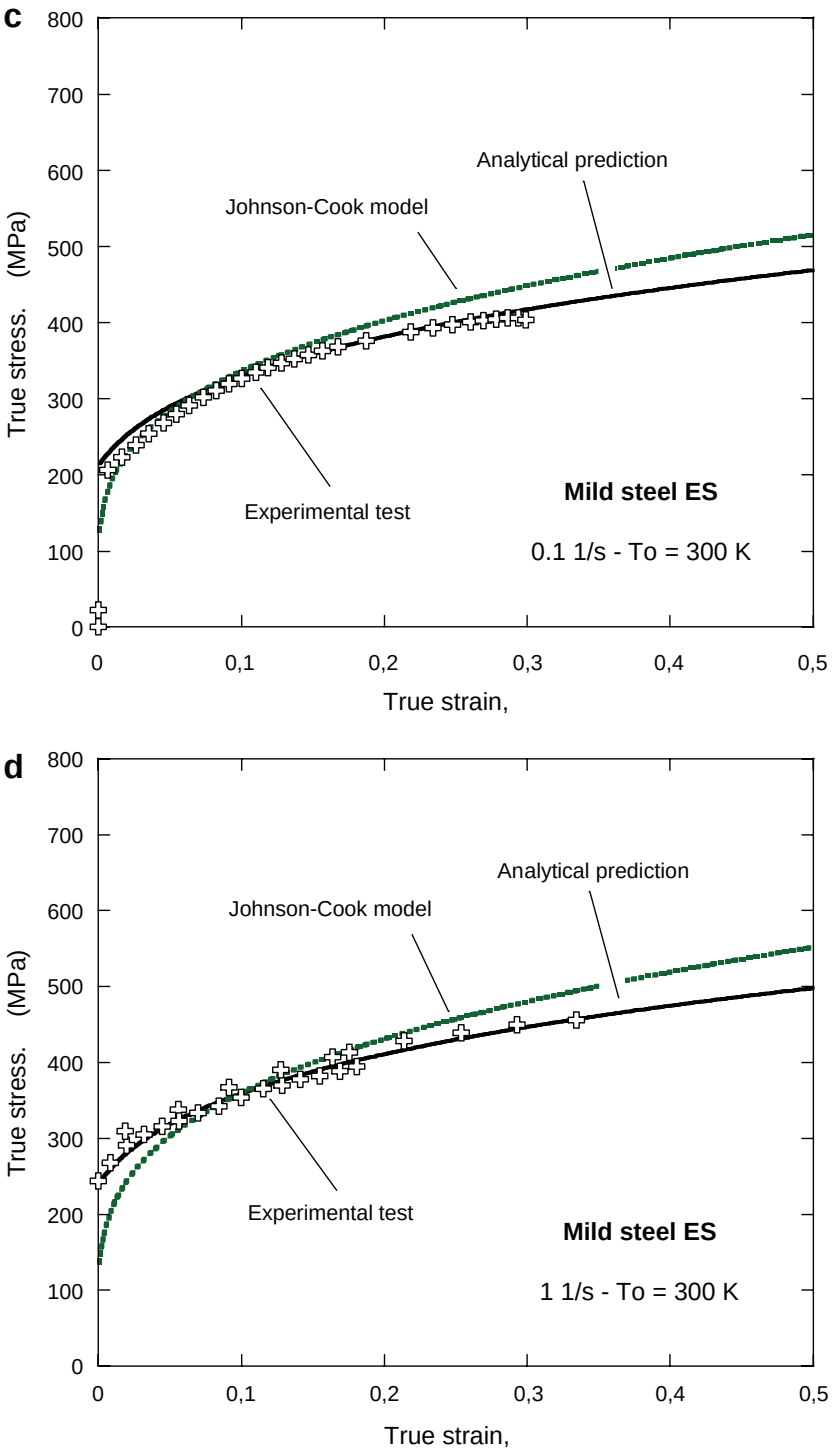

Fig. 6 (*continued*)

in which A, B, C and D are material constants, n is the strain hardening exponent, m is the temperature sensitivity, $\dot{\varepsilon}_0$ is the limit of the model in terms of strain rate, σ_{sta} is the reference stress level in quasi-static loading and $1/p$ defines the strain rate sensitivity, T^* is the normalized temperature. Moreover, the JC relation does not allow to predict correctly variations of the hardening rate θ which is introduced via the constant strain hardening exponent n, therefore it does not depend on strain rate and temperature, $\theta = K_0 n(\varepsilon_p)^{n\ 1}$, where K_0 is the

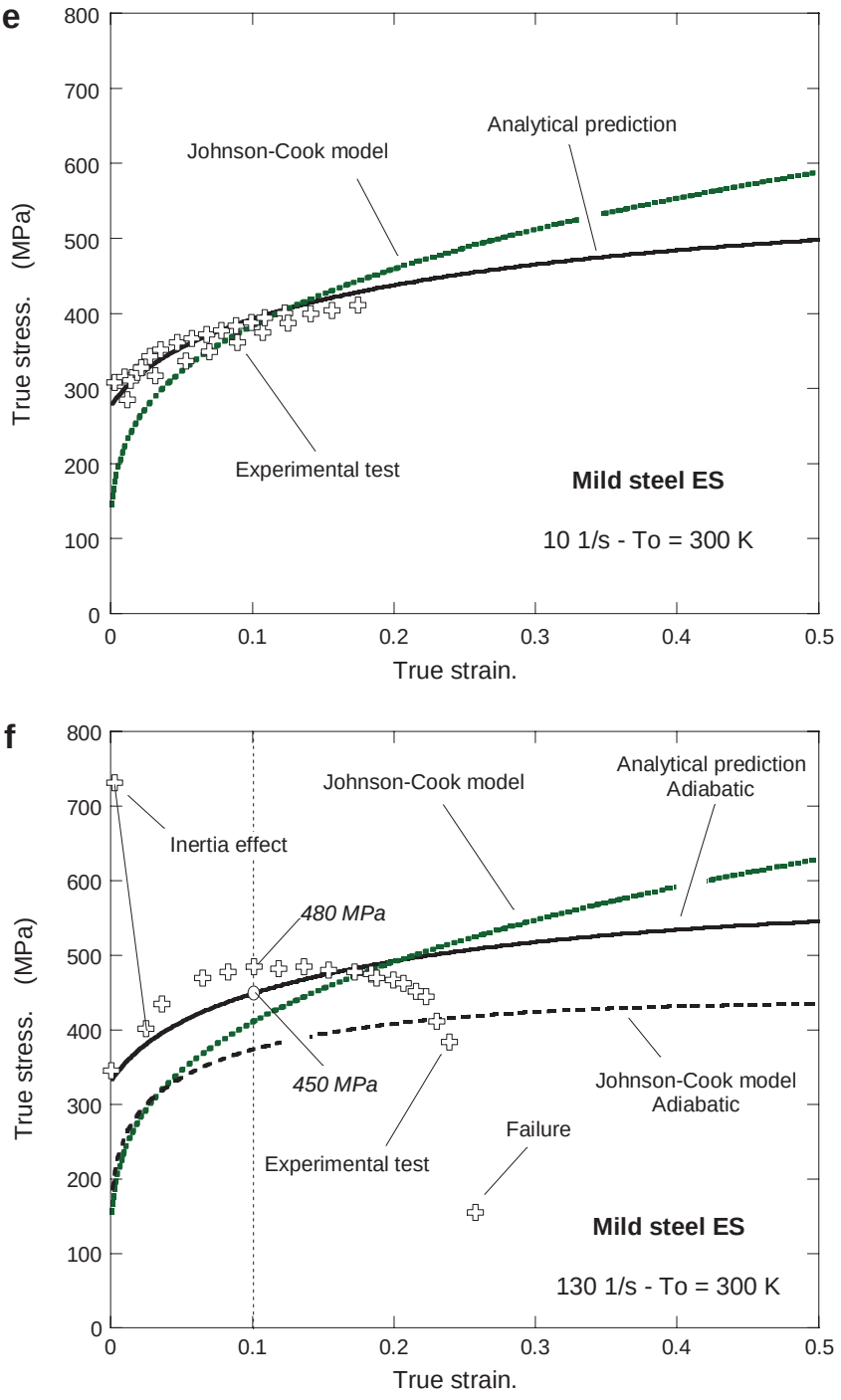

Fig. 6 (*continued*)

material constant obtained at $\dot{\varepsilon}_p =$ const and T^* const. An excessive strain hardening reached at large strains perturbs all analyses of dynamic instabilities at high strain rates.

The well known model of Zerilli–Armstrong is not included in this comparison since it is more physical and some background of materials science is necessary for a detailed discussion. However the parabolic strain hardening causes the same effects as mentioned above. It is well known that for the most BCC lattices the strain hardening rate θ depends on strain rate and temperature. Recently, a comparison was reported by Van Slycken et al. (2006), between the RK and JC constitutive relations for TRIP steel in terms of strain rate

Table 3
(a) Values of the parameters in RK model for mild steel ES, (b) values of the constants in the Johnson Cook model, (c) values of the constants in the Cowper Symonds model and (d) values of the constants in the Zhao model

(a) RK constitutive relation			
B_0	591.6	MPa	Modulus of plasticity
n_0	0.285	1	Strain hardening exponent
ε_0	1.8×10^{-2}	1	Initial strain
D_1	0.48	1	Material constant
v	0.2	1	Temperature sensitivity
σ_0^*	406.3	MPa	Effective stress at 0 K
m	2.8	1	Rate strain sensitivity
D_2	0.19	1	Material constant
E_0	212	GPa	Modulus of elasticity at 0 K
θ^*	0.59	1	Homologous temperature
T_m	1600	K	Melting point temperature
$\dot{\varepsilon}_{max}$	10^7	s^{-1}	Saturation strain rate
$\dot{\varepsilon}_{min}$	10^{-5}	s^{-1}	Minimal strain rate
C_p	470	J kg^{-1} 1 K^{-1}	Specific heat
β	0.9	1	Taylor Quinney's coefficient
ρ	7800	kg m^{-3}	Mass density
α	10^{-5}	K^{-1}	Thermal expansion
(b) Johnson Cook model			
A	57.27	MPa	Material constant
B	479.93	MPa	Material constant
n	0.316	1	Strain hardening exponent
C	*0.0362*	*1*	*Material constant*
$\dot{\varepsilon}_0$	10^{-3}	s^{-1}	Minimal strain rate
m	0.28	1	Temperature sensitivity
T_{room}	300	K	Room temperature
(c) Cowper Symonds Mourro (2002)			
D	40	s^{-1}	Material constant
P	5	1	Material constant
(d) Zhao Tanimura Mourro (2002)			
A	135	MPa	Material constant
B	435	MPa	Material constant
n	0.40	1	Strain hardening exponent
C	5.3	MPa	Material constant
D	11	MPa	Material constant
m	0.29	1	Rate strain sensitivity
k	0.25	1	Rate strain sensitivity
$\dot{\varepsilon}_0$	1	S^{-1}	Referential strain rate
E	48	MPa s	Material constant

sensitivity and strain hardening. The constitutive relation proposed by Zhao and Gary (1996), Eq. (21), developed initially for mild steel ES, was also plotted for comparisons in Fig. 3. This relation is sometimes pre-implemented in commercial FE codes and used to simulate behavior of crash-boxes in automotive industries.

$$\sigma\left(\varepsilon_p, \dot{\varepsilon}_p\right) = A + B\left(\varepsilon_p\right)^n + \left(C + D\left(\dot{\varepsilon}_p\right)^m \ln\left(\frac{\dot{\varepsilon}_p}{\dot{\varepsilon}_0}\right)\right) + E\left(\dot{\varepsilon}_p\right)^k \tag{21}$$

where A, B, C, D and E are material constants, n is the strain hardening exponent, m and k define strain rate sensitivity and $\dot{\varepsilon}_0$ is the limit of validity of the model. The difficulties with this relations stems from the negative value of D if $\dot{\varepsilon}_0 \geqslant \dot{\varepsilon}_p$. When numerical simulations are performed without proper attention, the third term in Eq. (21), leads to negative values of stress.

Comparison between all those constitutive relations and the results of experiment is shown in Fig. 3a, as a function of strain rate. A fairly good representation of the behavior is seen when using the RK constitutive

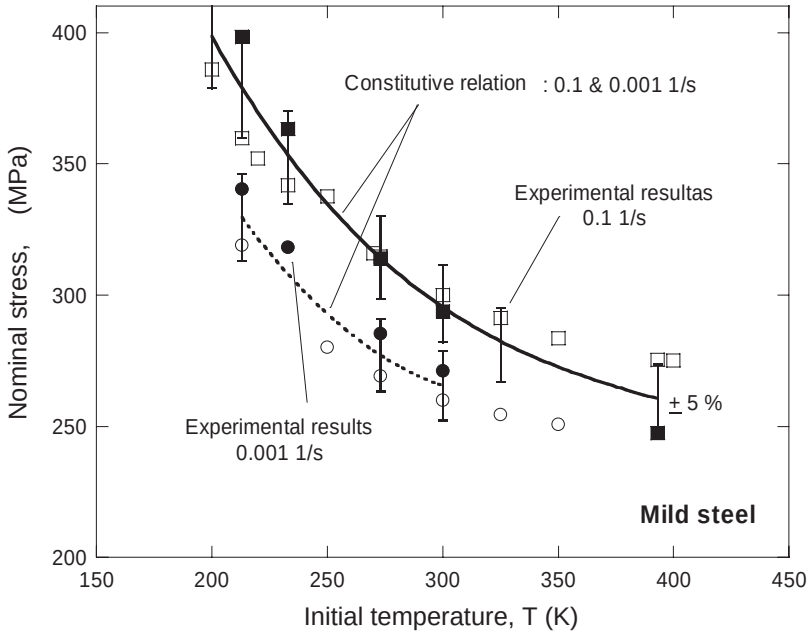

Fig. 7. Comparison of RK model predictions with experimental results at indicated strain rates with initial temperatures.

relation presented in this paper, whereas the Cowper–Symonds relation is not able to predict the rate effect correctly, if the strain rate is above $\dot{\varepsilon}_p > 10^{1}\ s^{-1}$. The same holds for the JC relation and that of Zhao and Gary (1996), which does not allow for a correct prediction of the rate sensitivity in the same range of strain rates. Moreover, the version introduced by Zhao and Gary (1996) does not include the strain rate and temperature effects in the strain hardening ($\theta = Bn(\varepsilon_p)^{n-1}$) as discussed previously. The problem found in the original version of the JC relation is directly related to the linear rate effect in the logarithmic scale, C is assumed constant and this is in disagreement with the experimental observations. Recently some authors have proposed a correction of this problem by introducing a complementary second term in the strain rate part of the JC relation, (Peixhino et al., 2003), but the problem persists at high strain rates when the temperature increase induces thermal softening of material due to adiabatic heating, an effect not well defined in the relation of Johnson and Cook (1983). Thus, if an energy criterion is used to define the failure of a structure, the failure appears quickly with the JC approximation, underestimating the mechanical resistance of the structure. A study of this effect on DP 600 steel was reported by Rusinek et al. (2004). A complementary advantage found in the RK constitutive relation is a possibility to take into account the stress behavior during a jump of strain rate from low to high or vice versa, Fig. 8a and b. Such behavior was observed experimentally by Klepaczko and Duffy (1982) for BCC metals submitted to a jump of strain rate at a specific plastic strain, characterized by a raise of stress in comparison to the original stress level at the same strain rate, can be to some extent modeled by the RK relation. Such behavior was interpreted by a microstructure evolution. More exactly, for a positive jump of strain rate ($\dot{\varepsilon}_p^1 \rightarrow \dot{\varepsilon}_p^2, \dot{\varepsilon}_p^1 < \dot{\varepsilon}_p^2$) the stress overshoot was observed in comparison to the $\sigma(\varepsilon)$ curve obtained with the same strain rate. On the contrary, the stress level was lower when a negative jump of strain rate was applied ($\dot{\varepsilon}_p^2 \rightarrow \dot{\varepsilon}_p^2$). In the present modeling such effect is not directly related to the microstructural evolution but is similar due to the adiabatic heating which produces similar phenomenon. Thus, in metallic materials with BCC microstructures such as mild steel, it is not necessary for engineering purposes to introduce a more complicated physical modeling but it is sufficient to introduce a more precise approximation of the strain hardening coupled with temperature and strain rate. This is not so for FCC metallic materials where the effect of microstructure evolution at different strain rates is more important. This is demonstrated during jumps of strain rate, Klepaczko and Duffy (1982), also Klepaczko and Chiem (1986). This point is important when a constitutive relation is applied in combination with an energetic failure criterion. In fact, the critical energy of failure can be well defined with the RK approach. Fig. 8c indicates a substantial difference during

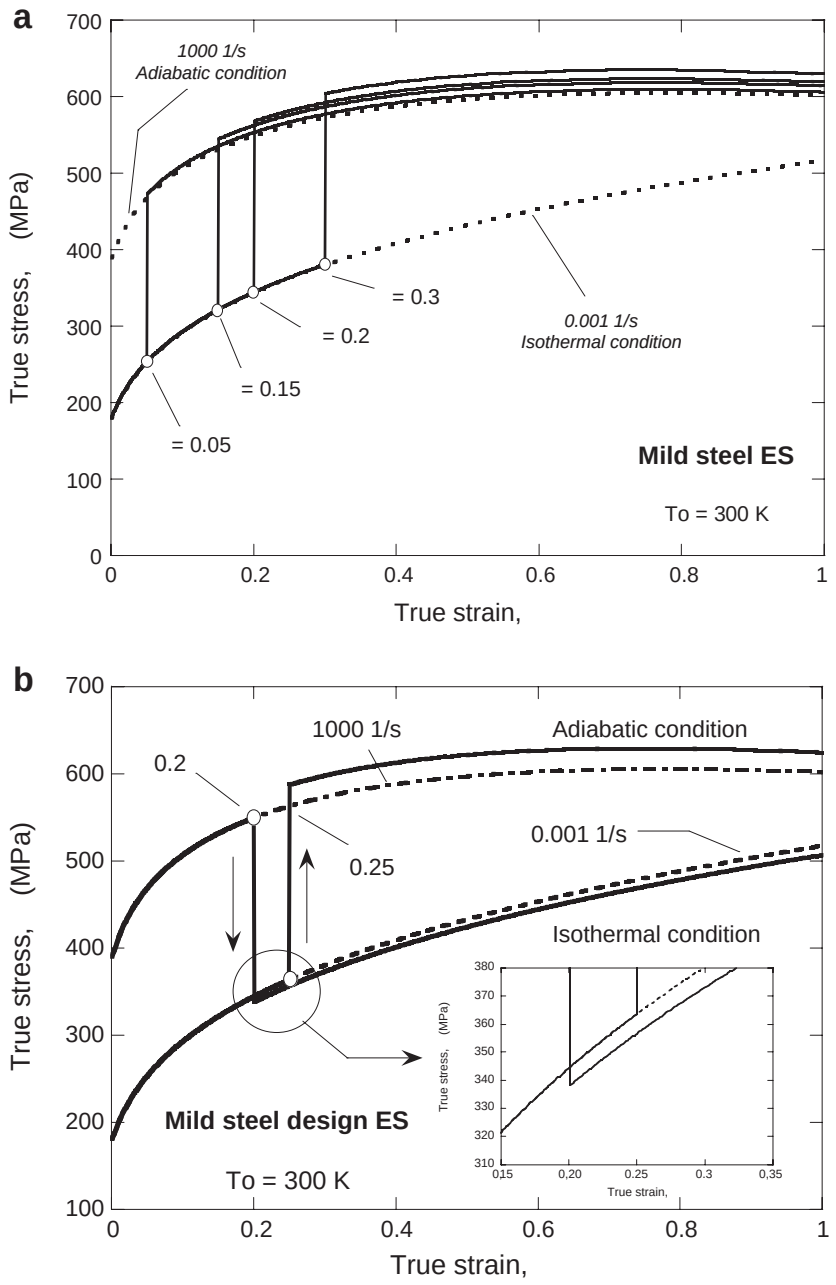

Fig. 8. (a) RK model predictions for a jump of strain rate from quasi static to dynamic rates for different plastic strain levels, (b) RK model predictions for a jump of strain rate from high to quasi static rate, (c) effect of pre deformation on the plastic work level.

the first stage of deformation after a positive strain rate jump, then the energy increases in comparison to that obtained by the continuous loading at the same strain rate.

4. Introduction of the RK constitutive relation into an integration algorithm for a numerical code

4.1. Implicit integration scheme of the constitutive model

The fundamental hypothesis of the whole 3D constitutive model, complementary to the Eqs. (9)–(16) are hypoelastic-plastic behavior, additive decomposition of the rate of deformation tensor commonly assumed for hypoelastic-plastic materials (Nemat-Nasser, 1982; Khan, 1998), isotropic elastic behavior defined through

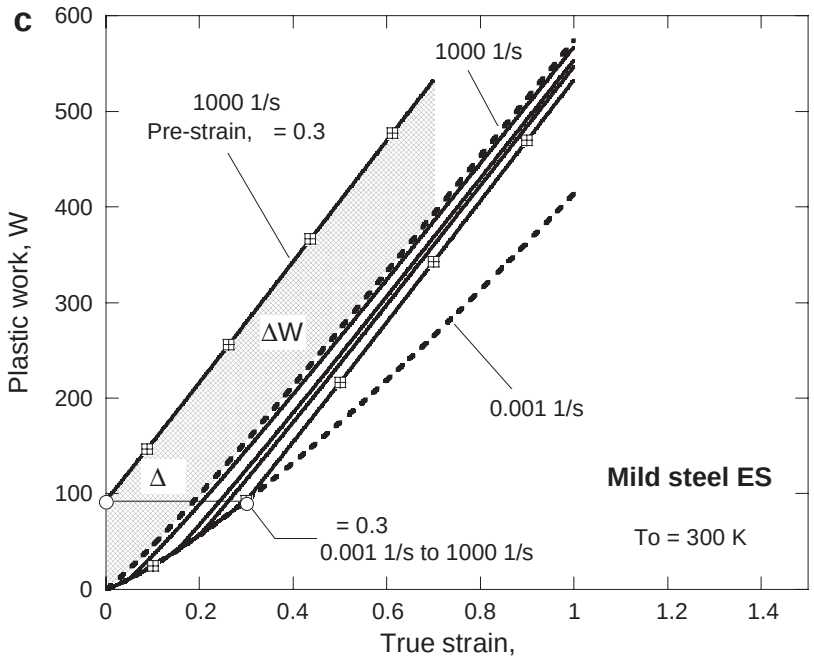

Fig. 8 (*continued*)

the generalized Hooke's law, J_2 plasticity with isotropic hardening, associated flow rule and isotropic thermal deformation. This set of non-linear equations should be integrated through a stress update algorithm. Within the finite element method, this integration process is local in space, that is, it occurs at quadrature points of the finite elements. The incremental integration of the constitutive model is regarded as a *strain-driven* process (Simo and Taylor, 1985) in which the increment of the total strain tensor at each quadrature point is given at a certain time, and both stress and state variables, defined as plastic strain, plastic strain rate and temperature, should be updated, preserving consistency if possible. That is, the stress must remain on the yield surface. With an explicit integration scheme such as the forward Euler, updated values of stress and state variables do not satisfy the yield condition at step $n+1$, so an implicit algorithm is required to avoid drift from the yield surface.

To solve this system of incremental equations, the implicit algorithm proposed by Zaera and Fernández-Sáez (2006) has been used and extended to the thermoviscoplastic hardening relation. The algorithm belongs to the class of methods called *return mapping algorithms*, Fig. 9, which are robust, accurate and widely used in practice (Simo and Ortiz, 1985; Simo and Taylor, 1986). The stress update is performed in two steps, an elastic predictor driven by an elastic increment in total strain leading to a trial stress state, and a plastic corrector which returns or projects the trial stress onto the revised yield surface in the direction specified by the plastic flow rule. The second step, which is performed iteratively, accounts for hardening or softening of the material

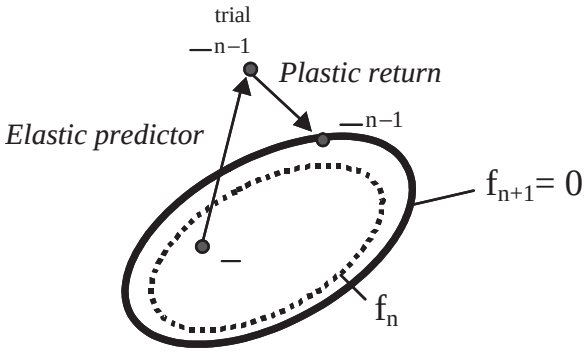

Fig. 9. Schematic representation of the return mapping algorithm used to satisfy the consistency equation.

(expansion or shrinkage of the yield surface). In order to preserve the physical meaning of the proposed thermoviscoplastic hardening relation, the proposed algorithm enforces, at every quadrature point, the equality of equivalent stress and yield stress for updated values of plastic strain, plastic strain rate and temperature. This follows the so-called consistency visco-plastic model, Eq. (22), due to Wang et al. (1997). Since the consistency is expected during plastic flow, the following equation is imposed

$$f^{n+1} = f\left(\underline{\underline{\sigma}}^{n+1}, \varepsilon_{\mathrm{p}}^{n+1}, \dot{\varepsilon}_{\mathrm{p}}^{n+1}, T^{n+1}\right) = \sigma^{n+1} - \sigma_y(\varepsilon_{\mathrm{p}}^{n+1}, \dot{\varepsilon}_{\mathrm{p}}^{n+1}, T^{n+1}) = 0 \tag{22}$$

This condition could be written as an equation, Eq. (23), where the only unknown is the increment of the plastic multiplier $\Delta\lambda$

$$f\left(\sigma_{\mathrm{trial}}^{n+1} - 3G\Delta\lambda, \lambda^n + \Delta\lambda, \frac{\Delta\lambda}{\Delta t}, T^n + \frac{\beta}{\rho^{n+1}C_{\mathrm{p}}}\left(\Delta\lambda\sigma_{\mathrm{trial}}^{n+1} - 3G\Delta\lambda^2\right)\right) = 0 \tag{23}$$

$\sigma_{\mathrm{trial}}^{n+1}$ being the equivalent stress at the trial elastic state. To solve Eq. (23) the Newton–Raphson iterative procedure is used. The linearization of the consistency condition, Eq. (23), and solving of the iterative increment in $\Delta\lambda$ leads to the following equation

$$\delta\Delta\lambda^k = \frac{f^k}{3G - \frac{\partial f}{\partial \varepsilon_{\mathrm{p}}}\Big|_k - \frac{1}{\Delta t}\frac{\partial f}{\partial \dot{\varepsilon}_{\mathrm{p}}}\Big|_k - \frac{\partial f}{\partial T}\Big|_k \frac{\beta}{\rho^{n+1}C_{\mathrm{p}}}\left(\sigma_{\mathrm{trial}}^{n+1} - 6G\Delta\lambda^k\right)} \tag{24}$$

The expressions for the different derivatives of the yield function are given in Appendix A. The plastic multiplier increment is revised after each iteration, and all state variables are updated when f^{n+1} is below a required value.

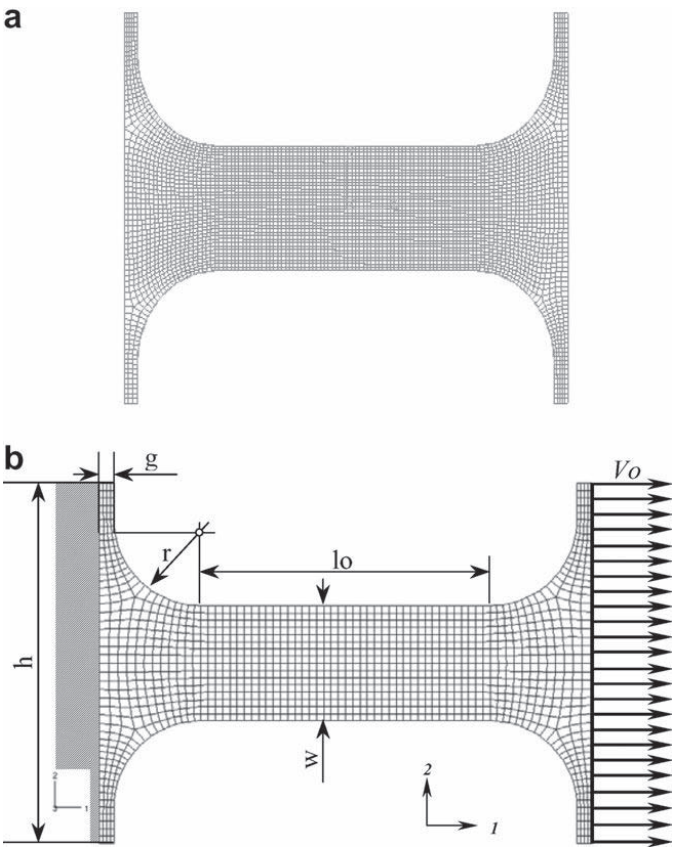

Fig. 10. (a) The optimal mesh used during numerical simulation and (b) boundary conditions applied in all numerical simulations presented.

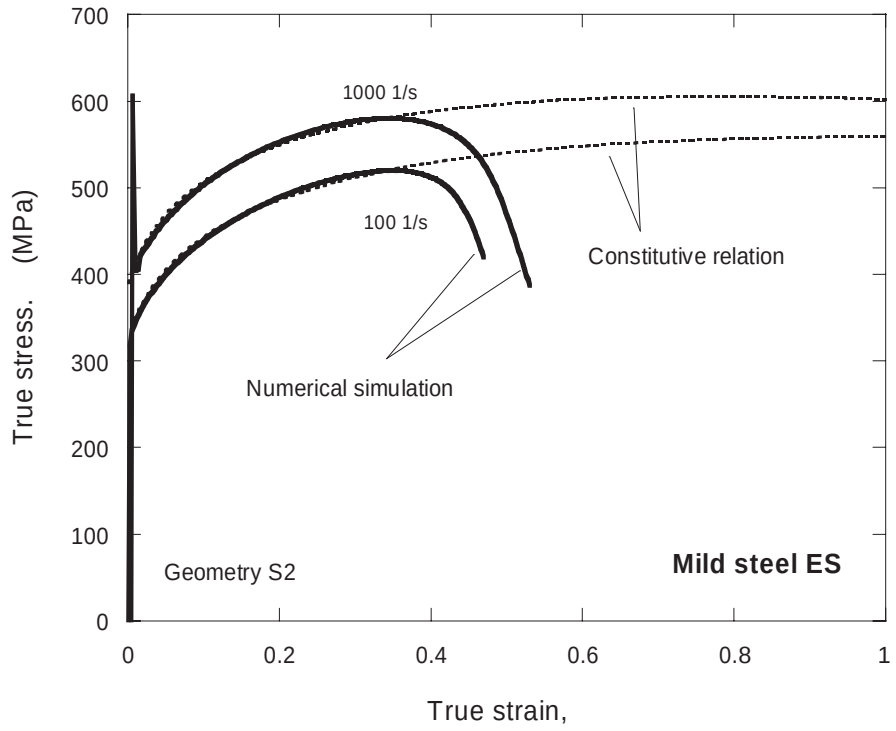

Fig. 11. Comparison between RK constitutive model predictions and numerical simulations using the modelling proposed for two strain rates.

To integrate the rate equations in a finite deformation frame preserving incremental objectivity, the equations were rewritten in the neutralized or corotational configuration (Simo and Taylor, 1985; Doghri, 2000; Hagege, 2004; Ponthot, 2002), therefore the complicated objective stress rate present in the elastic behavior law can be computed as a simple time derivative. Moreover, the rate equations defined above are form-identical in the neutralized configuration and a small deformation formulation could be used to integrate the thermoviscoplastic constitutive model.

4.2. Validation of the algorithm and the effect of elastic wave propagation and dynamic plasticity via RK constitutive relation

In order to validate the constitutive modeling by RK approach, several numerical simulations were performed of dynamic tension tests of sheet steel ES (Rusinek et al., 2005). The specimen shape and the meshes are depicted in Fig. 10a and b. The aim of this simulation was to compare the stress–strain curves obtained directly by analytic formulation with the numerical results obtained by reconstruction of the $\sigma - \varepsilon_{\mathrm{p}}|_{\dot{\varepsilon}_{\mathrm{p}}}$ curve. The results are shown in Fig. 11. The numerical simulation agrees well with the analytic predictions of the RK constitutive relation. The differences appear at large deformation when necking emerges. A simple reason is that the geometrical instability is not included in the analytic form of the constitutive relation. The material constants were identified for the homogeneous deformation field. An additional validation of the algorithm can be found in Rusinek and Zaera (2007), where the problem of dynamic ring expansion was simulated using the same numerical procedures.

5. Conclusions

By the combination of the original thermoviscoplastic constitutive relation and a new integration scheme that includes strain hardening, strain rate sensitivity and temperature effects, it is possible to simulate and study a variety of processes of dynamic loading and impact.

Complementary to the effort focussed on the development of sophisticated finite element tools and technical details of the finite element formulations, special attention must be paid to a kind of the constitutive relation which will allow to identify precisely the physical processes in dynamic plasticity. Those problems are well demonstrated by Rusinek and Zaera (2007) in the case of dynamic ring expansion. It was shown that the rate sensitive strain hardening strongly affects the number of fragments with the applied radial velocity. The constitutive relation presented in this paper may also be used to solve analytical problems as well as to be applied in a finite differences scheme. This is possible since the stress derivatives of all arguments can be found analytically (see Appendix, Eqs. (A.1)–(A.6)). With only eight fundamental material constants a wide range of strain rates and temperatures can be covered in sufficient precision. The most important innovation in the RK constitutive formulation is introduction of the rate and temperature strain hardening in the form of $n(\dot{\varepsilon}_p, T)$. Such modification enables numerical studies of all kinds of instabilities in dynamic plasticity.

Appendix A

Table A1
Values of the constants in RK model for IF steel and HSLA 65 steel

IF steel			HSLA 65 steel		
B_0	552.89	MPa	B_0	940	MPa
n_0	0.285	1	n_0	0.14	1
ε_0	1.8×10^{-2}	1	ε_0	1.8×10^{-2}	1
D_1	0.48	1	D_1	0.48	1
ν	0.2	1	ν	0.2	1
σ_0^*	406.3	MPa	σ_0^*	120	MPa
m	2.8	1	m	2.8	1
D_2	0.19	1	D_2	0.19	1
E_0	212	GPa	E_0	212	GPa
θ^*	0.59	1	θ^*	0.59	1
T_m	1600	K	T_m	1600	K
$\dot{\varepsilon}_{max}$	107	s^{-1}	$\dot{\varepsilon}_{max}$	107	s^{-1}
$\dot{\varepsilon}_{min}$	10^{-5}	s^{-1}	$\dot{\varepsilon}_{min}$	10^{-5}	s^{-1}
C_p	470	J kg^{-1} K^{-1}	C_p	470	J kg^{-1} K^{-1}
β	0.9	1	β	0.9	1
ρ	7800	kg m^{-3}	ρ	7800	kg m^{-3}
α	10^{-5}	K^{-1}	α	10^{-5}	K^{-1}

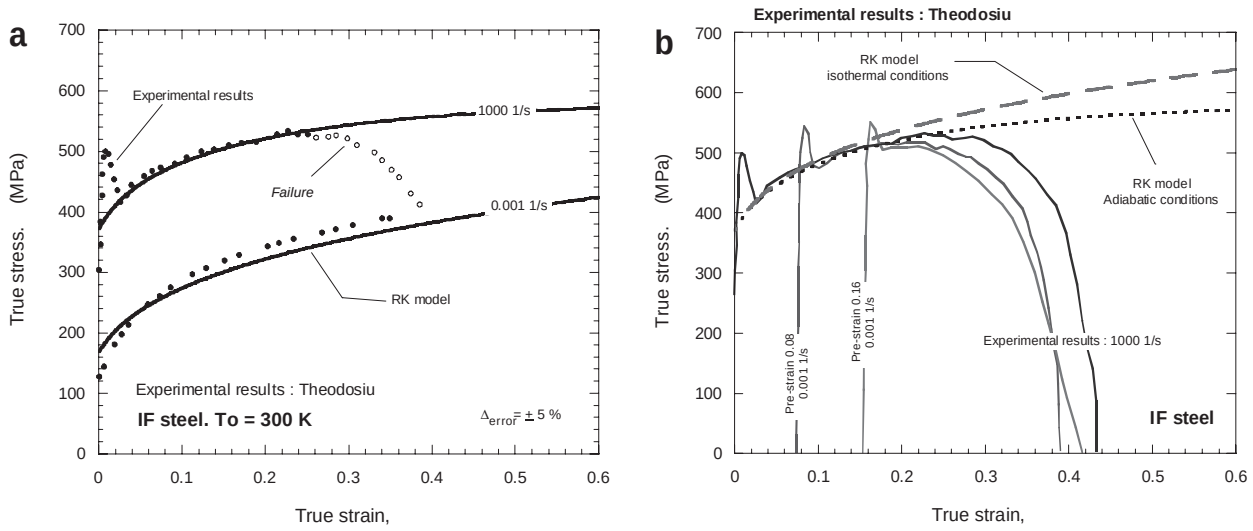

Fig. A1. Comparison between RK constitutive model predictions and experimental results for IF steel, Uenishi and Teodosiu (2004): (a) strain rate sensitivity and (b) quasi static pre deformation effect for dynamic loading.

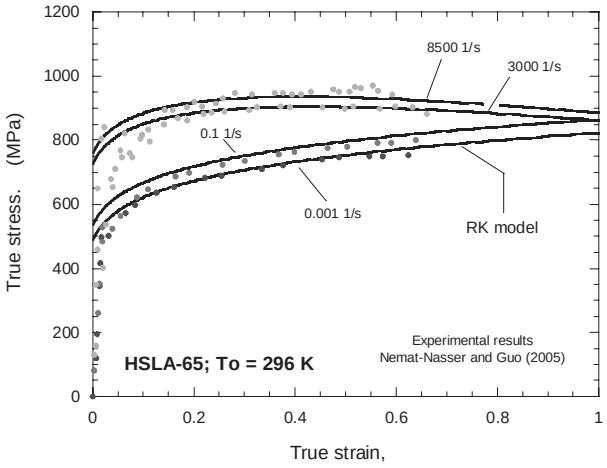

Fig. A2. Comparison between constitutive model predictions and experimental results of Nemat Nasser and Guo (2005) for a wide range of strain rates.

$$\left.\frac{\mathrm{d}\sigma_\mu}{\mathrm{d}\varepsilon^p}\right|_{\dot{\varepsilon}_\mathrm{p},T} = B(\dot{\varepsilon}_\mathrm{p},T)n(\dot{\varepsilon}_\mathrm{p},T)(\varepsilon_0+\varepsilon_\mathrm{p})^{n(\dot{\varepsilon}_\mathrm{p},T)\ \ 1} \tag{A.1}$$

$$\left.\frac{\mathrm{d}\sigma_\mu}{\mathrm{d}\dot{\varepsilon}_\mathrm{p}}\right|_{\dot{\varepsilon}_\mathrm{p},T} = B(\dot{\varepsilon}^p,T)(\varepsilon_0+\varepsilon_\mathrm{p})^{n(\dot{\varepsilon}_\mathrm{p},T)}\left[\frac{v(\varepsilon_0+\varepsilon_\mathrm{p})}{\dot{\varepsilon}_\mathrm{p}\log\left(\frac{\dot{\varepsilon}_\mathrm{max}}{\dot{\varepsilon}_\mathrm{p}}\right)}-\frac{n_0D_2\ln(\varepsilon_0+\varepsilon_\mathrm{p})}{\dot{\varepsilon}_\mathrm{p}T_\mathrm{m}}\right] \tag{A.2}$$

$$\left.\frac{\mathrm{d}\sigma_\mu}{\mathrm{d}T}\right|_{\varepsilon_\mathrm{p},\dot{\varepsilon}_\mathrm{p}} = -B(\dot{\varepsilon}_\mathrm{p},T)(\varepsilon_0+\varepsilon_\mathrm{p})^{n(\dot{\varepsilon}_\mathrm{p},T)}\left[\frac{v}{T}+\frac{n_0D_2}{T_\mathrm{m}}\log\left(\frac{\dot{\varepsilon}_\mathrm{p}}{\dot{\varepsilon}_\mathrm{min}}\right)\ln(\varepsilon_0+\varepsilon_\mathrm{p})\right] \tag{A.3}$$

$$\left.\frac{\mathrm{d}\sigma^*}{\mathrm{d}\dot{\varepsilon}_\mathrm{p}}\right|_{\dot{\varepsilon}_\mathrm{p},T} = \frac{mD_1}{\dot{\varepsilon}_\mathrm{p}\ln(10)}\left(\frac{T}{T_\mathrm{m}}\right)\sigma_0^*\left[1-D_1\frac{T}{T_\mathrm{m}}\log\left(\frac{\dot{\varepsilon}_\mathrm{max}}{\dot{\varepsilon}_\mathrm{p}}\right)\right]^{m^*\ \ 1} \tag{A.4}$$

$$\left.\frac{\mathrm{d}\sigma^*}{\mathrm{d}T}\right|_{\varepsilon^p,\dot{\varepsilon}_\mathrm{p}} = -\frac{mD_1}{T_\mathrm{m}}\log\left(\frac{\dot{\varepsilon}_\mathrm{max}}{\dot{\varepsilon}_\mathrm{p}}\right)\sigma_0^*\left[1-D_1\frac{T}{T_\mathrm{m}}\log\left(\frac{\dot{\varepsilon}_\mathrm{max}}{\dot{\varepsilon}_\mathrm{p}}\right)\right]^{m^*\ \ 1} \tag{A.5}$$

$$\frac{\mathrm{d}E}{\mathrm{d}T} = -E_0\exp\left[\theta^*\left(1-\frac{T_\mathrm{m}}{T}\right)\right]\left(\frac{1}{T_\mathrm{m}}+\frac{\theta^*}{T}\right) \tag{A.6}$$

References

ABAQUS Explicit Version 6.4, User's manual, ABAQUS Inc., Richmond, USA, 2004.

Batra, R.C., Kim, C.H., 1990. Effect of viscoplastic flow rules on the initiation and growth of shear bands a high strain rates. J. Mech. Phys. Solids 38, 859 874.

Bodner, S.R., Partom, Y., 1975. Constitutive equations for elastic viscoplastic strain hardening materials. ASME J. Appl. Mech. 42, 385 389.

Campbell, J.D., Ferguson, W.G., 1970. The temperature and strain rate dependence of the shear strength of mild steel. Philos. Mag. 21, 63 82.

Conrad, H., 1964. Thermally activated deformation of metals. J. Metals 16, 582.

Considère, M., 1885, L'emploi du fer de l'acier dans les constructions, Mémoire no. 34, Annales des Ponts et Chaussées, Paris, pp. 574 575.

Cowper, G.R., Symonds, P.S., 1952, Strain hardening and strain rate effects in the impact loading of cantilever beams, Brown Univ., Div. of Appl. Mech., Report no. 28.

Doghri, I., 2000. Mechanics of Deformable Solids: Linear and Non linear, Analytical and Computational Aspects. Springer, Berlin (Chapter 16).

Follansbee, P.S., Kocks, U.F., 1988. A constitutive description of the deformation of copper based on the use of the mechanical threshold stress as an internal state variable. Acta Met. 36, 81 93.

Gilman, J.J., 1968. Dislocation dynamics and response of materials to impact. Appl. Mech. Rev. 21, 767 783.

Hagege, B., 2004, Simulation du comportement mécanique des renforts fibreux en grandes transformations: application aux renforts tricots, Ph.D. thesis, ENSAM de Paris.

Hodowany, J., Ravichandran, G., Rosakis, A.J., Rosakis, P., 2000. Partition of plastic work into heat and stored energy in metals. Exp. Mech. 40, 113 123.
Hoge, K.G., Mukherjee, A.K., 1977. The temperature and strain rate dependence of the flow stress of tantalum. J. Mater. Sci. 12, 1666 1672.
Johnson, G.R., Cook, W.H., 1983, A constitutive model and data for metals subjected to large strains, high strain rates and high temperatures. In: Proceedings of 7th International Symposium on Ballistics, pp. 541 547.
Khan, A., 1998. Continuum Theory of Plasticity. Wiley, New York (Chapter 8).
Klepaczko, J.R., 1968. Generalized conditions for stability in tension test. Int. J. Mech. Sci. 10, 225 237.
Klepaczko, J.R., 1975. Thermally activated flow and strain rate history effects for some polycrystalline FCC metals. Mater. Sci. Engng. 18, 121 135.
Klepaczko, J.R., 1981, The relation of thermally activated flow of BCC metals and ferritic steels to strain rate history and temperature history effects, Materials Research Laboratory, Brown University, Technical Report DMR 79 23257/2.
Klepaczko, J.R., 1987, Modelling of structural evolution at medium and high strain rates, FCC and BCC metals. In: Constitutive Relations and Their Physical Basis, Roskilde, Risö Natl. Lab., pp. 387 392.
Klepaczko, J.R., 1994. General approach to rate sensitivity and constitutive modelling of FCC and BCC metals. Impact Effects of Fast Transient Loadings. A.A. Balkema, Rotterdam, pp. 3 45.
Klepaczko, J.R., Chiem, C.Y., 1986. On rate sensitivity of FCC metals, instantaneous rate sensitivity and the rate sensitivity of strain hardening. J. Mech. Phys. Solids 14, 29.
Klepaczko, J.R., Duffy, J., 1982. History effects in polycrystalline BCC metals and steel subjected to rapid changes in strain rate and temperature. Arch. Mech. 34, 419 436.
Kocks, U.F., 1976. Laws for work hardening and low temperature creep. J. Eng. Mater. Technol. 98, 76 85.
Kocks, U.F., Argon, A.S., Ashby, M.F., 1975. Thermodynamics and kinetics of slip. In: Progress in Materials Science, vol. 19. Pergamon Press, New York.
Larour, P., Baumer, A., Bleck, W., 2005, High strain rate tensile testing of modern car body steels. In: SCT05 Conference Proceeding, Wiesbaden, Germany, pp. 1 8.
Larour, P., Rusinek, A., Klepaczko, J.R., Bleck, W., 2007, Effects of strain rate and identification of material constants for three automotive steels, Steel Res. Int., in press.
Liang, R., Khan, A.S., 1999. A critical review of experimental results and constitutive models for BCC and FCC metals over a wide range of strain rates and temperatures. Int. J. Plasticity 15, 963 980.
Macdougall, D., 2000. Determination of the plastic work converted to heat using radiometry. Exp. Mech. 40, 298 306.
Meyers, M.A., Benson, D.J., Vohringer, O., Kad, B.K., Xue, Q., Fu, H., 2002. Constitutive description of dynamic deformation: Physically based mechanisms. Mater. Sci. Engng. A 322, 194 216.
Molinari, A., Ravichandran, G., 2005. Constitutive modeling of high strain rate deformation in metals based on the evolution of an effective microstructural length. Mech. Mater. 37, 737 752.
Mourro, P, 2002, Etude du comportement dynamique des tôles d'acier pour le calcul de crash, Ph.D. thesis, Ecole Polytechnique de Paris, France.
Nemat Nasser, S., 1982. On finite deformation elastoplasticity. Int. J. Solids Struct. 18, 857 872.
Nemat Nasser, S., Guo, W.G., 2005. Thermomechanical response of HSLA 65 steel plates. Mech. Mater. 37, 379 405.
Nowacki, W.K., 2001, Dynamic simple shear of sheets at high strain rates. In: Nowacki, W.K., Klepaczko, J.R. (Eds.), New Experimental Methods in Material Dynamics and Impact, Series: Trends in Mechanics of Materials, vol. 3, pp. 309 336.
Peixhino, N., Jones, N., Pinho, A., 2003. Experimental and numerical study in axial crushing of thin walled sections made at high strength steels. J. Phys. IV 110, 717 722.
Ponthot, J.F., 2002. Unified stress update algorithms for the numerical simulation of large deformation elasto plastic and elasto viscoplastic processes. Int. J. Plast. 18, 91 126.
Rusinek, A., 2000, Modélisation thermoviscoplastique d'une nuance de tôle d'acier aux grandes vitesses de déformation. Etude expérimentale et numérique du cisaillement, de la traction et de la perforation, Ph.D. thesis, University of Metz, France.
Rusinek, A., Klepaczko, J.R., 2001. Shear testing of sheet steel at wide range of strain rates and a constitutive relation with strain rate and temperature dependence of the flow stress. Int. J. Plasticity 17, 87 115.
Rusinek, A., Zaera, R., 2007. Finite element simulation of steel ring fragmentation under radial expansion. Int. J. Impact Eng. 34, 799 822.
Rusinek, A., Gadaj, P., Klepaczko, J.R., Nowacki, W.K., 2004. Experimental study of mild steel sheets, DP and TRIP: Proposition of a constitutive relation. Matériaux & Techniques 5 6, 1 10.
Rusinek, A., Zaera, R., Klepaczko, J.R., Cheriguenne, R., 2005. Analysis of inertia and scale effects on dynamic neck formation during tension of sheet steel. Acta Mater. 53, 5387 5400.
Seeger, A., 1957. The mechanism of glide and work hardening in face centered cubic and hexagonal close packed metal. In: Fisher, J.C. (Ed.), Dislocations and Mechanical Properties of Crystals. J. Wiley, New York.
Simo, J.C., Ortiz, M., 1985. A unified approach to finite deformation elastoplastic analysis based on the use of hyperelastic equations. Comp. Meth. Appl. Mech. Eng. 51, 241 245.
Simo, J.C., Taylor, R.I., 1986. A return mapping algorithm for plane stress elastoplasticity. Int. J. Numer. Meth. Eng. 22, 649 670.
Simo, J.C., Taylor, R.I., 1985. Consistent tangent operators for rate independent elastoplasticity. Comp. Meth. Appl. Mech. Eng. 48, 101 118.
Uenishi, U., Teodosiu, C., 2004. Constitutive modelling of the high strain rate behaviour of interstitial free steel. Int. J. Plast. 20, 915 936.

Van Slycken, J., Verleysen, P., Degrieck, J., Bouquerel, J., 2006. Constitutive equations for multiphase TRIP steels at high rates of strain. J. Phys. IV France 134, 69 74.

Wang, V.M., Sluys, L.J., de Borst, R., 1997. Viscoplasticity for instabilities due to strain softening and strain rate softening. Int. J. Num. Meth. Eng. 40, 3839 3864.

Zaera, R., Fernández Sáez, J., 2006. An implicit consistent algorithm for the integration of thermoviscoplastic constitutive equations in adiabatic conditions and finite deformations. Int. J. Solids Struct. 43, 1594 1612.

Zerilli, F.J., Armstrong, R.W., 1987. Dislocation mechanics based constitutive relations for material dynamics calculations. J. Appl. Phys. 61, 1816 1825.

Zhao, H., Gary, G., 1996. The testing and behaviour modelling of sheet metals at strain rates from 10^{-4} to 10^{4} s^{-1}. Mater. Sci. Eng. A 207, 46 50.